small methods
www.small-methods.com

Nanothermometer Based on Polychlorinated Trityl Radicals Showing Two-Photon Excitation and Emission in the Biological Transparency Window: Temperature Monitoring of Biological Tissues

Nerea Gonzalez-Pato, Davide Blasi, Domna M. Nikolaidou, Francesco Bertocchi, Jesús Cerdá, Francesca Terenziani, Nora Ventosa, Juan Aragó, Andrea Lapini, Jaume Veciana, and Imma Ratera**

Nanothermometers are emerging probes as biomedical diagnostic tools. Especially appealing are nanoprobes using NIR light in the range of biological transparency window (BTW) since they have the advantages of a deeper penetration into biological tissues, better contrast, reduced phototoxicity and photobleaching. This article reports the preparation and characterization of organic nanoparticles (ONPs) doped with two polychlorinated trityl radicals (TTM and PTM), as well as studies of their electronic and optical properties. Such ONPs having inside isolated radical molecules and dimeric excimers, can be two-photon excited showing optimal properties for temperature sensing. Remarkably, in TTM-based ONPs the emission intensity of the isolated radical species is unaltered increasing temperature, while the excimer emission intensity decreases strongly being thereby able to monitor temperature changes with an excellent thermal absolute sensitivity of 0.6–3.7% K^{-1} in the temperature range of 278–328 K. The temperature dependence of the excimeric bands of ONPs are theoretically simulated by using electronic structure calculations and a vibronic Hamiltonian model. Finally, TTM-doped ONPs as ratiometric NIR-nanothermometers are tested with two-photon excitationwith enucleated pig eye sclera, as a real tissue model, obtaining a similar temperature sensitivity as in aqueous suspensions, demonstrating their potential as NIR nanothermometers for bio applications.

1. Introduction

During the last years, we have assisted to a rising interest on the implementation of substituted trityl radicals as emitting species in electroluminescent devices.[1,2] Owing to their doublet electronic configuration, such trityl radicals allow overcoming the problems associated to the exciton statistics in OLEDs,[3,4] without the need of using expensive phosphorescent emitters.[5,6] This is not the only interesting aspect of this class of open-shell molecules, since their unique absorption and emission properties can be proficiently employed in other photoluminescence applications, especially in bioimaging.[7,8] Indeed, many substituted trityl radicals present an intense absorption in the near-UV region (≈ 380 nm), and a low-intensity absorption corresponding to a $D_0 \rightarrow D_1$ transition close to 550 nm.[9] Such radicals are usually weakly emitting species in solution, with values of fluorescence quantum yield (ϕ_F) of about 0.02, caused

N. Gonzalez-Pato, D. Blasi, N. Ventosa, J. Veciana, I. Ratera
Institut de Ciència de Materials de Barcelona (CSIC)/CIBER-BBN
Campus de la UAB
Bellaterra, Barcelona E-08193, Spain
E-mail: vecianaj@icmab.es; iratera@icmab.es

The ORCID identification number(s) for the author(s) of this article can be found under https://doi.org/10.1002/smtd.202301060

DOI: 10.1002/smtd.202301060

D. Blasi
Department of Chemistry
University of Bari Aldo Moro
Bari 70125, Italy

D. M. Nikolaidou, F. Bertocchi, F. Terenziani, A. Lapini
Department of Chemistry, Life Sciences and Environmental Sustainability
University of Parma
Parco Area delle Scienze 17/a, Parma 43124, Italy

J. Cerdá, J. Aragó
Instituto de Ciencia Molecular
Universitat de València
Catedrático José Beltrán 2
Paterna 46980, Spain

A. Lapini
LENS
European Laboratory for Non-Linear Spectroscopy
Via Nello Carrara 1, Sesto Fiorentino (Fi) 50019, Italy

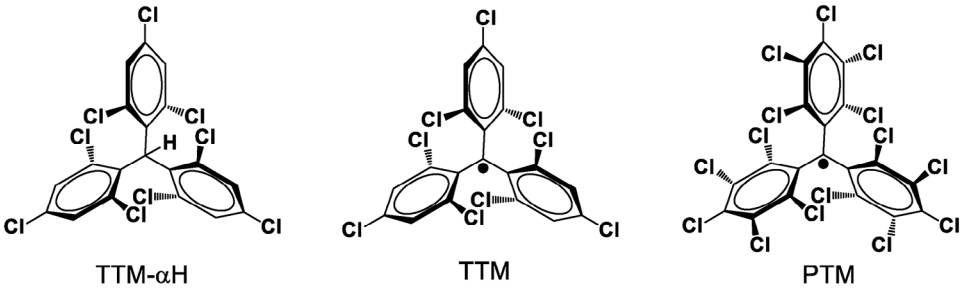

Scheme 1. Molecular structures of TTM-αH, and of TTM and PTM radicals.

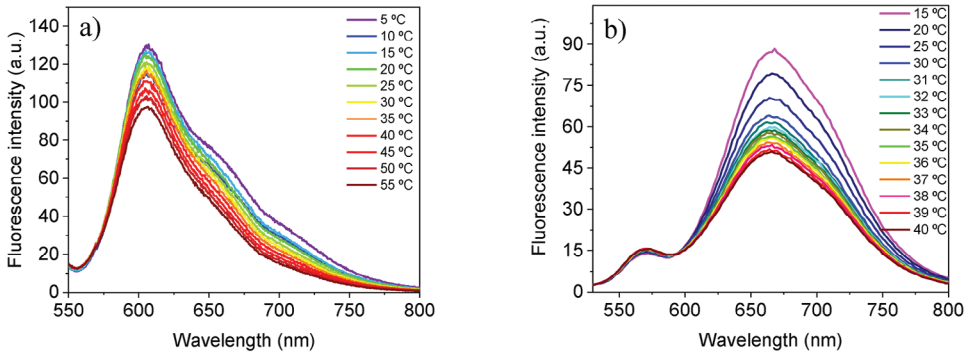

Figure 1. Emission spectra at different temperatures of water suspensions of ONPs containing a 26% in mol of radical for a) PTMd-ONPs excited at λ_{exc} 385 nm and b) TTMd-ONP excited at λ_{exc} 377 nm.[13e.]

by the low oscillator strength associated to the relevant transition from the Kasha's state (the lowest excited electronic state) to the ground state, and the consequent prolonged radiative lifetime (≈400 ns at room temperature and ≈300 ns at 77 K)[10–16] that makes the internal conversion (IC) mechanisms favored. Quantum yield is proportional to the radiative decay constant k_r, which in turns depends on the oscillator strength. Once immobilized in diluted frozen solutions at 77 K, such trityl radicals, and in a more general way carbon-centred free radicals, exhibit values of ϕ_F up to 0.7–0.8.[10,11] Nevertheless, in the condensed solid-state they are strongly affected by the aggregation-caused quenching (ACQ) phenomenon that decreases the fluorescence quantum yield.[1,11,17]

Recently, we have demonstrated that dilution of the tris(2,4,6-trichlorophenyl)methyl radical (TTM, **Scheme 1**) into optically-neutral organic rigid matrices, such as polymers or solid nanoparticles, improves the luminescence properties, the photostability, and promotes the formation of red/NIR-emitting excimers.[10,18] In addition, we have demonstrated that nanoparticles made of the optically neutral tris(2,4,6-trichlorophenyl)methane (TTM-αH, **Figure 1**b) and doped with TTM can be used as ratiometric fluorescent nanothermometers for bio applications.[18] These nanoparticles (TTMd-ONPs), when excited at 377 nm, exhibit a dual emission due to the presence of the radical monomer and excimer species. The monomer emission appears at 572 nm with an almost temperature-independent intensity, while the excimer emission appears around 665 nm and its intensity decreases with the temperature raising. TTMd-ONPs show an excellent thermal absolute sensitivity (S_a) of 0.6–3.7% K^{-1} in a wide temperature range (from 278 to 328 K). The absolute sensitivity, S_a, is estimated according to Equation (1), where $\partial Q = \partial[I_M/I_E]$ is the fluorescence quenching for a given temperature change (∂T), being I_M and I_E the intensity maxima of the monomer and excimer emissions, respectively. TTMd-ONPs also displays an excellent temperature-sensitive emission reversibility and a minimum temperature resolution of 0.3 ° (See Supporting Information). Moreover, TTMd-ONPs are not cytotoxic and their ratiometric output, the ratio between the emission intensities of monomer and excimer, I_M/I_E, is not affected either by different aggregation levels of the nanoparticles or by changes on pH and ionic strength that may occur under physiological conditions. Such nanoparticles are therefore able to measure temperature changes at the nanoscale by the ratiometric output of each individual particle or their small aggregates.

$$S_a = \left|\frac{\partial Q}{\partial T}\right| \times 100\%, \ \left[\% \cdot K^{-1}\right] \quad (1)$$

Finally, in vivo thermometry experiments made with *Caenorhabditis elegans* worms indicated that TTMd-ONPs can be used as fluorescence imaging probes and to monitor the temperature changes inside the worms from 278 to 313 K with a high sensitivity.[18] All such results indicate the considerable potential applications of polychlorinated trityl radical-based ONPs in biological nanothermometry. However, to expand this application it is convenient to shift the excitation wavelength of

A. Lapini
Istituto Nazionale di Ricerca Metrologica (INRIM) strada della Cacce 91
Torino 10135, Italy

radical doped ONPs to the first biological transparency window (BTW) at the NIR region (650–950 nm), allowing to decrease the cytotoxicity of UV excitation light and at the same time to achieve a higher penetration-depth inside biological tissues for possible in vivo investigations with such ONPs.[19,20] In this context, it should be mentioned that open-shell fluorophores based on push-pull trityl radical derivatives have shown outstanding two-photon absorption cross sections,[21,22] while no studies have been reported on isolated and excimeric forming polyhalogenated trityl radicals.

Here we investigate if aqueous suspensions of ONPs doped with two polychlorinated trityl radicals (Scheme 1), TTM and PTM (perchlorotriphenylmethyl), can be two-photon excited in the NIR region yielding concurrent emission in the first BTW region as well. Thus, we prepared and investigated the optical properties and behavior of such doped ONPs, namely TTMd-ONPs and PTMd-ONPs, as nanoprobes for NIR thermometry since the use of light in the range of the first BTW could provide the abovementioned advantages for their use as nanothermometers in tissues studies.[22] The choice of PTM radical as possible fluorescent probe for two-photon nanothermometry was suggested by the fact that the PTM radical in solution exhibits a more red-shifted absorption and emission compared to the less chlorinated TTM species. TTM-αH ONPs showed spherical morphology and high colloidal stability even at high temperature with an impressive biocompatibility. The resulting photoluminescence properties of PTMd-ONPs were compared with those of our previous reported TTM-based nanoparticles, TTMd-ONPs.

2. Results and Discussion

Before studying the photoluminescence properties of PTM and TTM radical-doped ONPs, the absorption and emission of isolated PTM radical molecules in THF at room temperature and in 2-MeTHF at 77 K (Figure S1 and Table S1, Supporting Information) were revisited. PTM radical in THF solution at r.t. presents a maximum of absorption at 385 nm, a maximum of emission at 610 nm (16.393 cm^{-1}, with λ_{exc} = 377 nm), with a value of ϕ_F of 0.02, and an excited-state lifetime of about 9 ns (Figure S2, Supporting Information). Using the simple relation $\phi_F = k_r/(k_r + k_{nr}) = k_r\tau$, where k_r is the radiative rate constant, k_{nr} the non-radiative rate constant and τ the excited-state lifetime, we obtain $k_r = 2 \times 10^6$ s^{-1} and $k_{nr} = 103 \times 10^6$ s^{-1}. In the glassy 2-MeTHF solution at 77 K, the PTM radical shows a strong improvement of ϕ_F, achieving a value of 0.54, a lower value than TTM for which a ϕ_F of 0.72 was observed under the same conditions.[11] The maximum of absorption was peaked at 387 nm while the emission was blue-shifted of 605 cm^{-1}, with a maximum at 589 nm (16.998 cm^{-1}) and two vibronic peaks at 640 nm (15.625 cm^{-1}) and 703 nm (14.225 cm^{-1}). By contrast, in absorption only minor variations occur with respect to r.t., namely a narrowing of the vibronic bands due to the decrease of the inhomogeneous broadening. Assuming that k_r is not sensitively affected by changes in temperature and viscosity,[23,24] the excited-state lifetime at 77 K amounts to 250 ns, more than one order of magnitude longer than in solution, which is consistent with values reported for other trityl radicals in frozen matrices.[12,14] A similar considerable enhancement of ϕ_F was also obtained dispersing PTM in poly(methylmethacrylate) (PMMA) films (see Supporting Information section), achieving a value of ϕ_F of 0.19 and an average lifetime of 100 ns.[10,11] These results suggested the possibility to obtain good luminescence properties using PTM radical as a dopant of ONPs, i.e., in PTMd-ONPs. Hence, PTMd-ONPs using TTM-αH as the inert matrix and containing different amounts of PTM radical (0.5, 3, 6.5, 13, 26, and 50% in mol.) were prepared using the re-precipitation method (see Supporting Information section).[11] TTM-αH, the hydrogenated analogue of the TTM radical, was chosen as the host because it is transparent in the visible region and allows generating ONPs with good colloidal properties, and offers, due to its structure, a receptive environment to the highly chlorinated radical guest molecules.[11] Dynamic light scattering (DLS) analysis of the resulting PTMd-ONPs aqueous suspensions gave average hydrodynamic diameters in the 50–90 nm range with polydispersity indexes (PDI) $<$ 0.16 and Z-potentials of ≈−42 mV for all the samples, indicative of good colloidal stability (Figure S3, Supporting Information). Transmission electron microscopy (TEM) images confirmed the DLS measurements revealing the spherical morphology of the ONPs and their monomodal size distribution (Figure S3, Supporting Information).

Absorption spectra of PTMd-ONPs suspensions in water are affected by light scattering due to their nanoscopic size, especially in the near-UV region where the radical-doped ONPs present the maximum of absorption (Figure S4, Supporting Information). In order to correct the scattering component, the absorption spectra of suspensions of ONPs with pure TTM-αH with comparable sizes and size distributions were used as a reference to determine the scattering-correction functions (Figure S4, Supporting Information), since TTM-αH is completely transparent in the 300–800 nm range.[11,25] The scattering-corrected absorption spectra of the PTMd-ONP suspensions (Figure S5, Supporting Information) are quite similar to the spectrum of PTM in THF, confirming the good quality of the correction method. The absorbance value of PTMd-ONP suspensions after the scattering correction were used for the evaluation of ϕ_F values. The confinement of the PTM radical in a rigid environment, like in the ONPs, leads to a significant enhancement of ϕ_F, due to the reduction of radiationless mechanisms of excited states decay. Indeed, the luminescence quantum yield amounts to ϕ_F = 0.40 in the case of the 0.5% PTMd-ONPs and to 0.15 for the 3% PTMd-ONPs, corresponding to enhancements of the luminescence of one order of magnitude with respect to the THF solution at r.t. (ϕ_F = 0.02). When increasing further the amount of radical doping, an efficient aggregation-caused quenching (ACQ) of the emission is observed, leading to a halving of the luminescence efficiency when doubling the radical concentration, with an almost completely emission quenching in the case of the 50% PTMd-ONPs (Figure S6, Supporting Information) affecting also the fluorescence lifetimes (Figure S7 and Table S2, Supporting Information).

Emission spectra of low-doped (0.5–6.5%) PTMd-ONPs are very similar to the emission spectrum of PTM radical in THF solution (Figure S6, Supporting Information), while for higher concentrations the band broadens on the low-energy side because of the appearance of a shoulder whose intensity increases as the radical doping level is increased. Based on the results obtained for TTM-doped ONPs,[11] this red-shifted shoulder is attributed

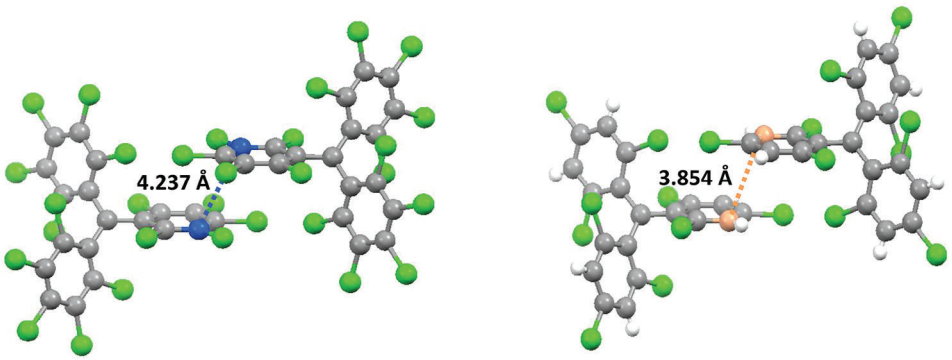

Figure 2. Left, crystallographic structure of the PTM radical with a symmetry C2/c,[26] Right, crystallographic structure of TTM radical with a symmetry C2/c.[27] For both radicals the minimum distance between two neighbouring molecules is along *meta* carbon positions, represented in blue and orange, respectively.

to a very weak excimeric emission band located close to 700 nm (Figure 1).

The much lower intensity of the excimeric band in the case of PTMd-ONPs with respect to what was observed for TTMd-ONPs (where, for the 26% doped sample the emission was purely excimeric)[11] suggests that the presence of bulky chlorine atoms at the *meta* positions of trityl radicals may be responsible for this difference. In fact, X-ray data of single crystals of TTM and PTM radicals[25–27] reveal the trend of forming dimers in solid state with minimum distances between the two aromatic carbon atoms at the *meta* positions of parallel phenyl rings of two neighboring molecules (**Figure 2**). While this distance is of 3.854 Å for the TTM radical, in the case of PTM it is larger, amounting to 4.237 Å because of the presence of chlorine atoms in *meta* positions hindering a closer approach. This fact observed at the condensed solid state could explain the lower tendency of PTM molecules to form excimeric species in radical doped ONPs.

In order to explain the temperature dependence of the excimeric bands of both types of ONPs, we simulated the emission properties of the monomers and dimers of PTM and TTM species. Prior to the theoretical discussion, it is interesting to recall that excimeric states in molecular dimers generally imply an important mixing between Frenkel (FE) and charge-transfer (CT) excited states together with a significant structural relaxation (mostly intermolecular motions).[28–30] That FE-CT mixing is proportional to the hole and electron transfer integrals and the energy position of the FE and CT excited states. While FE states are less sensitive to intermolecular motions, the energy position of CT states can considerably vary by intermolecular vibrations due to the relevance of the electrostatic contribution in these CT states. On the other hand, transfer integrals are also very sensitive to intermolecular dispositions because they strongly depend on the orbital overlap. Hence, thermal intermolecular motions around the crystal structure may induce an important fluctuation of the transfer integrals and an energy (de)stabilization of the CT states.[31] This effect would be expected to be stronger for TTM compared to PTM since crystal dimers in TTM exhibit shorter intermolecular contacts than PTM.

Turning our attention to the electronic structure calculations, we have performed time-dependent density functional theory (TD-DFT) calculations for the radical monomers and dimers of PTM and TTM species using the optimally-tuned ωB97X-D/6-31G** level of theory (see Figures S8,S9 (Supporting Information) for further details). As structural relaxation for both PTM and TTM dimers within their corresponding ONPs (i.e., PTMd-ONPs and TTMd-ONPs) are hindered in some degree, we have started analyzing the nature of the lowest-energy excited states for PTM and TTM monomers and dimers at the crystal structures (Table S3, Supporting Information). For both PTM and TTM dimers, the first two singlet electronic transitions are predicted energetically close to the first electronic transition ($D_0 \rightarrow D_1$) of the monomers (447 and 443 nm, for PTM and TTM radicals, respectively). Therefore, the first two singlet excited states of PTM and TTM dimers are of FE-type character and can be mainly described as the symmetric and antisymmetric interaction of the first doublet excited state of the radical monomer. The small energy difference between these two singlet excited states for PTM and TTM dimers comes from the small excitonic coupling (−1.2 and 0.5 meV for PTM and TTM dimers). The comparison of Table S3 (Supporting Information) also reveals that the first CT excited states are found to be higher in energy compared to the lowest-energy FE-type states for PTM and TTM (0.64 and 0.39 eV, respectively). That is in line with the shorter intermolecular distance found for TTM compared to PTM ($d(C_{meta}\text{-}C_{meta})$ 3.854 and 4.237 Å, respectively) that would promote a more favorable electrostatic interaction and, thus, an energy stabilization of the CT states. These findings already suggest that TTM dimers may exhibit upon relaxation an excited state with a significant FE-CT mixing (excimeric state) and, consequently, TTM would display an enhanced excimeric emission band compared to PTM as experimentally observed (Figure 1).

To investigate further the effect that small intermolecular motions cause in the excited states energies, we have computed energy difference maps (i.e., $\Delta E_{CT\text{-}FE}$) for PTM and TTM dimers as a function of small intermolecular displacements (Figures S10,S11, Supporting Information). For TTM, relatively small intermolecular displacements along the z and x directions starting from the crystal disposition, where the two aromatic rings are interacting more strongly (e.g., in the positive 0.3–0.5 Å range), are enough to stabilize the CT states with respect to the lowest-energy FE-type states by 0.1–0.15 eV. This effect is even stronger at larger displacements in the x-z bisector by 0.75 and 1.0 Å ($\Delta E_{CT\text{-}FE}$ of 0.19 and 0.24 eV, respectively). A similar effect has been predicted for PTM (Figure S10, Supporting

Information) although the energy $\Delta E_{CT\text{-}FE}$ values have been always obtained higher (> 0.5 eV) than those obtained for TTM. These outcomes therefore support that TTM is more prone to display an excimeric emission compared to PTM.

Based on the above electronic structure calculations for PTM and TTM monomers and dimers, we have also parameterized a vibronic Hamiltonian similar to that recently proposed by Spano and co-workers[30] to simulate the emission spectra of PTM and TTM monomers and dimers (see Table S5, Supporting Informationfor further details). For both PTM and TTM radical monomers (Figure S12, Supporting Information), the simulated emission spectra are almost insensitive to temperature variations in the 5–55 °C range and exhibit structured emission bands with vibronic peaks at 448, 467, and 493 nm (461, 479, and 511 nm) for PTM (TTM). For PTM and TTM dimers, we have simulated emission spectra at different temperatures (5–55 °C) and with two different $\Delta E_{CT\text{-}FE}$ conditions ($\Delta E_{CT\text{-}FE} = 0.0$ eV and $\Delta E_{CT\text{-}FE} = -0.20$ eV). For the former resonance condition ($\Delta E_{CT\text{-}FE} = 0.0$ eV), the simulated emission spectra for both PTM and TTM dimers are still similar to those predicted for the monomers and hardly temperature-dependent. That situation significantly changes at the $\Delta E_{CT\text{-}FE} = -0.20$ eV condition where the CT state is energetically below the FE-like state. The emission bands are now highly sensitive to temperature (Figure S12, Supporting Information). For PTM, a dominant unstructured and red-shifted band (excimeric band) at 529 nm compared to the monomer-like band (454 nm) emerges at low temperatures whereas a monomer-like emission band is the most intense band with an important tail at 523 nm (excimeric band) at high temperatures. The simulated emission spectrum at r.t. for PTM dimer is in reasonably agreement with that experimentally registered for the PTMd-ONPs doped with a 26% (Figure 1a; Figure S12, Supporting Information), which exhibits an extended emission band, however the intensity of the excimeric band with temperature barely changes, reproducing qualitatively what was obtained experimentally. For TTM dimer, the emission spectra pattern for all the temperatures is characteristic of an excimer with a dominant broad and red-shifted emission band. That excimeric band decreases in intensity with the increase of temperature in line with the experimentally observed emission pattern for TTM (Figure 1b; Figure S12, Supporting Information).[11] Therefore, our theoretical model can satisfactory explain the experimental changes of emission spectra at different temperatures.

As already mentioned before, a relevant drawback of polychlorinated trityl radical-based ONPs for their use as nanothermometers is the need of using near-UV excitation light to efficiently excited them, which is potentially cytotoxic and also leads to low penetration depth into biological tissues. In order to overcome both problems, we tested the two-photon excitation of TTM and PTM radicals in solution. **Figure 3** shows the normalized one-photon absorption and emission spectra (black, with $\lambda_{exc} = 380$ nm) and the absolute two-photon absorption spectra (Red lines, expressed in Goeppert-Mayer (GM) units) of TTM and PTM radicals in THF solution. Such spectra indicate that both radicals can be excited via two-photon absorption (2PA) at NIR wavelengths of 810 and 860 nm, with 2PA cross-sections (σ_2) of 17 and 6 GM for TTM and PTM radicals, respectively (See Supporting Information for 2PA cross-section evaluation). The emission spectra of TTM and PTM obtained upon two-photon excitation are superimposable to the corresponding one-photon-excited emission spectra. Although the properties mentioned above are relevant for bio-imaging applications of both radical-based ONPs, the weakness of the excimer band of PTMd-ONPs as well as the lower 2PA cross-section, in comparison with that of TTMd-ONPs, limits their use as efficient ratiometric 2PA nanothermometers. This limitation made us focus on the study of 2PA nanothermometers based on TTMd-ONPs.

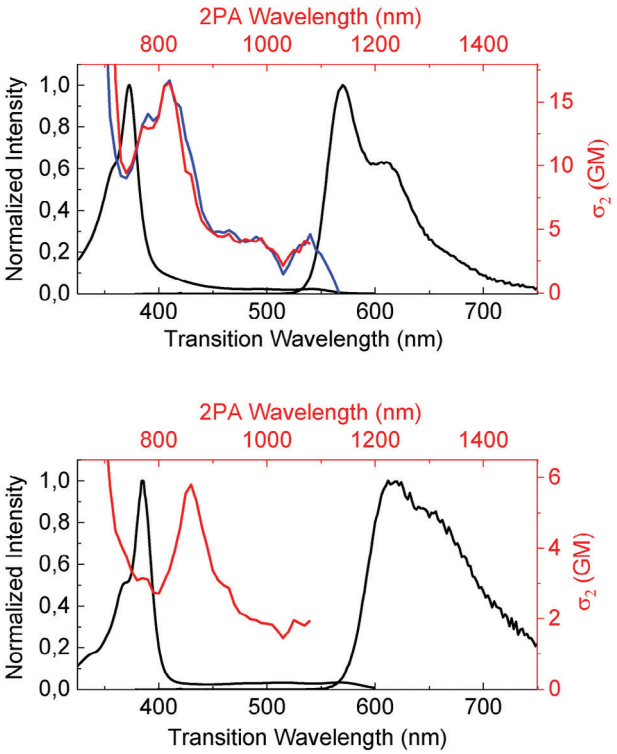

Figure 3. One-photon absorption and emission spectra (normalized, black lines) and two-photon absorption spectrum (Red line, right and top scale) of TTM (top panel) and PTM (bottom panel) in THF. Blue line (top panel): normalized two-photon excitation spectrum of TTM-ONPs.

The efficiency of TTMd-ONP as an effective NIR-to-red/NIR nanoreporter of local temperature (i.e., using NIR light for the excitation and getting red/NIR emission) was investigated in solution and on a biological substrate depositing a dispersion of TTMd-ONP on a slice of hydrated sclera from porcine eye. The sclera tissue was chosen as the suitable candidate to test the two-photon excited fluorescence (2PEF) of TTMd-ONPs due to its very low self-fluorescence (**Figure 4**).[32] As a first step, we performed one-photon excited fluorescence measurement, with $\lambda_{exc} = 380$ nm, of a diluted suspension of TTM-ONPs (ca., 0.002 mM) in a cryostat at the 5–35 °C temperature range. Normalized fluorescence spectra are reported in **Figure 5**a. Fluorescence spectra are characterized by two bands that have been attributed, respectively, to the monomer and excimer emissions.[11] The ratio between the green-shaded and the red-shaded area of emission spectra ($Q = A_G/A_R$) as a function of temperature during a heating and cooling cycle was calculated and shown in Figure 5c. The ratio between these two areas was chosen as a metrics for the ratiometric output instead of using the

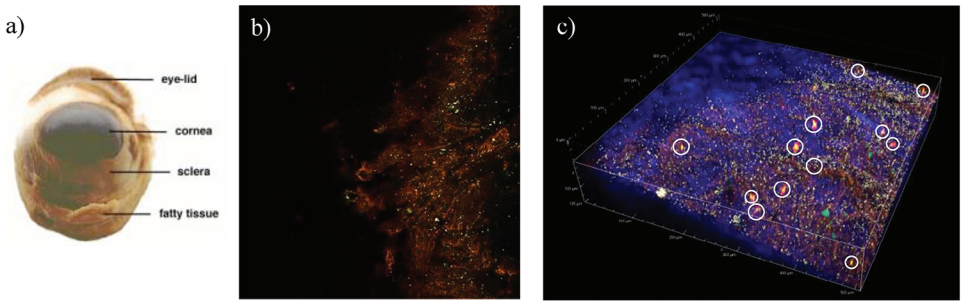

Figure 4. a) Porcine eye, indicating its main parts, among them the sclera tissue.[32] b) microscope image of a slice of porcine sclera tissue containing the TTMd-ONPs and c) 3D image of the sclera tissue showing the TTM-ONPs (white circles) penetration along the *z*-axis.

intensities at the emission maxima of monomer and excimers. Despite the availability of the entire emission spectrum in the one-photon excited fluorescence measurements (Figure 5a), we chose to use the ratio between the green-shaded and the red-shaded area to be consistent with the ratio that we are forced to use in the two-photon excited experiment (Figure 5b, due to the limited accessible spectral range).

The aim of such "one-photon-excitation" preliminary measurements was to obtain a reference correlation curve between the fluorescence monomer/excimer ratio and temperature to compare with the 2PEF measurement (Figure 5b). The results, reported in Figure 5c, show an almost linear correlation in the 5–35 °C temperature range from which a thermal absolute sensitivity S_a = 0.52–0.73 or mean 0.62 ± 0.06% K^{-1} and S_r= 1.080–1.095 or mean 1.088 ± 0.004% K^{-1} were obtained (see Equations (S1), Supporting Information). 2PEF measurements were conducted with a Nikon A1R MP+ Upright multiphoton microscope coupled with a femtosecond pulsed laser source (Coherent Chameleon-Discovery, 80 fs, 80 MHZ, 660–1320 nm). The microscope is equipped with a spectrograph (composed by a prism, as dispersing element, and a photomultiplier tube as a detector) capable of acquiring the spectrum of the fluorescence emitted by the sample with a resolution of 10 nm within the 435–645 nm spectral range. Unfortunately, due to limitations of our equipment, the spectral range cannot be expanded up to 800 nm. To measure the spectrum, the microscope records a

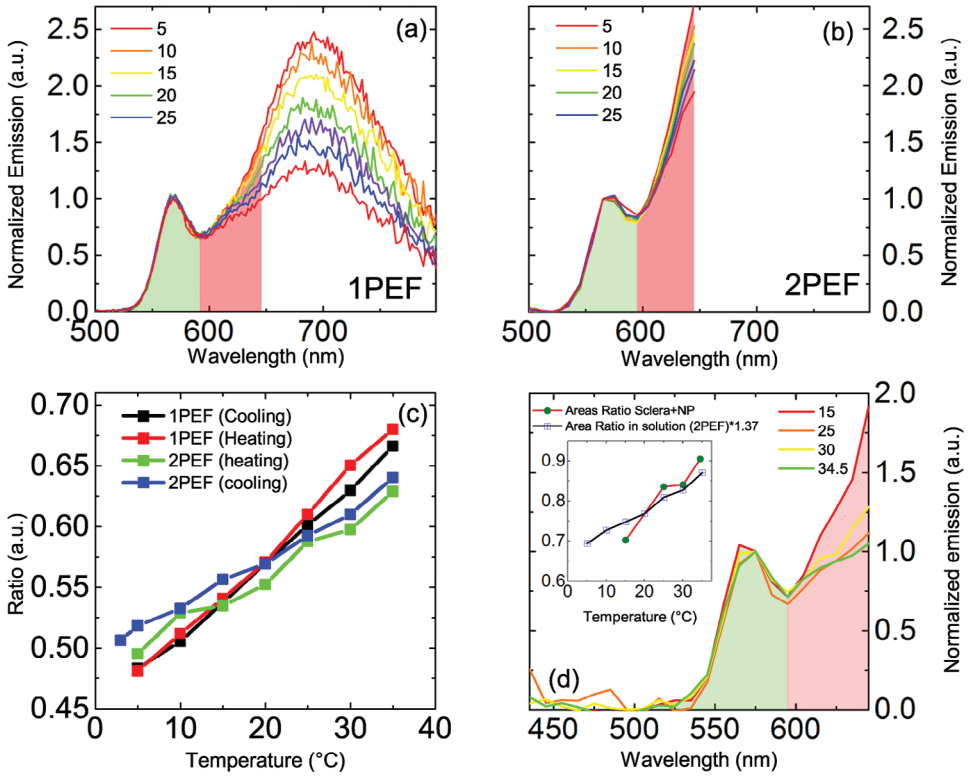

Figure 5. a) One-photon-excited and b) two-photon-excited emission spectra of TTM-ONPs water suspension as function of temperature (in°C). c) Evolution of the ratio between green-shaded and red-shaded area with the temperature. d) Two-photon-excited emission spectra of TTM-ONPs dispersed on a slice of porcine sclera tissue. Inset: Area Ratio as a function of temperature of TTM-ONPs on sclera tissue (green dots and red line) in comparison with TTM-ONPs suspension of Figure 5c) multiplied by a scaling factor (1.37).

series of images (in this case a low spatial resolution, 64 × 64 pixels, is enough) each one at a different emission wavelength: 22 images to cover the 435–645 nm spectral range with 10 nm steps. Then, each point of the spectral profile is obtained by integrating (over all the pixels) the signal from each image. The measurements on the TTM-ONPs suspension were performed on a 1 mm thick cuvette in contact with a base plate whose temperature was controlled owing to a thermostat with an external circulator and monitored with an external thermo-couple. 2PEF spectra are reported in Figure 5b and the areas ratios were calculated as well (Figure 5c), showing S_a = 0.24–0.64 or mean 0.41 ± 0.1% K^{-1} and S_r = 0.48–0.99 or mean 0.7 ± 0.1% K^{-1} (see Equations (S1), Supporting Information) that are in a very nice agreement with the one-photon-excited results, demonstrating the potential of TTM-ONPs as NIR-to-red/NIR nanothermometers for bio applications. In the second phase of our work, we investigated, with the help of the apparatus described before, the 2PEF response of the TTM-ONPs dispersed on a few mm thick slice of hydrated sclera tissue from porcine eye. The sclera tissue, previously hydrated, was treated with a water suspension containing TTM-ONPs for half an hour before the measurement session. The same suspension of TTM-ONPs was used as contact medium between the objective (25× Nikon CFI APO LWD Objective, 420–1400 nm, 1.10 NA, 2.0 mm WD) and the tissue surface. Since fluorescence is excited by exploiting a 2PA process, it will occur with appreciable probability only where the photon density is maximum, i.e., in the focus produced by the objective. This allows to eliminate any interference due to the presence of TTM-ONPs in the contact solution between the focal plane and the objective surface, as well as to gain the typical 3D spatial resolution intrinsic of nonlinear optical techniques.

In these conditions, we measured the emission spectrum of TTM-ONPs on the sclera surface following the procedure described before. The procedure has been repeated for various temperatures and the results are displayed in Figure 5d. Following the same approach formerly adopted, the ratio between the green-shaded and the red-shaded area of the emission spectra as a function of temperature has been also represented (Figure 5d inset). A slightly different response of the TTM-ONPs as a function of temperature was observed from water suspension and sclera surface. Nevertheless, the temperature trend is still linear and the two sets of measurements can be correlated by using a simple scaling factor. Therefore, the outcomes obtained for this sclera tissue model demonstrate that TTMd-ONPs are excellent NIR-to-red/NIR nanothermometers with promising capabilities for bio applications.

3. Conclusions

Polychlorinated trityl radicals TTM and PTM can be one- and two-photon excited in solution exhibiting acceptable two-photon absorption (2PA) cross-sections of 17 and 6 GM, respectively. This result provides the possibility to prepare NIR-based ratiometric nanothermometers made of organic nanoparticles (ONPs) doped with such radicals, containing the radical molecules in form of monomer and of dimeric excimers. The emission intensity of ONPs doped with a small amount of TTM and PTM radicals (i.e., isolated radical species), is unaltered varying temperature when excited with one-photon absorption (1PA). In contrast, the excimer emission intensity decays with the temperature increase allowing to monitor temperature changes by a ratiometric approach. The excimer intensity changes with temperature exhibited by TTM radical-doped ONPs are more pronounced than those of ONPs doped with PTM, in line with the theoretical simulations and the closer intermolecular distances of TTM-based excimers. Accordingly, TTMd-ONPs show an excellent temperature absolute sensitivity of 0.6–3.7% K^{-1} in the 278–328 K temperature range. This excellent property, together with a good 2PA cross sections, made TTM-ONPs excellent candidates for NIR-to-red/NIR temperature sensing. This was confirmed by measuring the emission spectra of a water suspension of TTM radical-based ONPs in the 5–35 °C temperature range with 2PA, using an excitation wavelength of 810 nm, which show very similar ratiometric output signals as those obtained with 1PA excitation at 380 nm and similar thermal absolute sensitivities of S_a= 0 .24–0.64 % K^{-1}. Up to now there are no all-organic nanothermometers like the ones described in this work: the highest sensitivity values in temperature sensing are only obtained with rare earths, which present some biocompatibility issues. To the best of our knowledge, one of the highest values reported of sensitivity is 9% K^{-1}, but this high sensitivity is only achieved at cryogenic temperatures, around 100 K.[33,34] The average reported values of sensitivity around physiological conditions are of the order of 2–3% K^{-1}[35,36] but usually not associated with NIR excitation. NIR excitation is instead possible with our systems which present promising maxima values of 3.7% K^{-1} in one-photon excitation and 0.64% K^{-1} in two-photon excitation.

Finally, and as a proof of concept, the use of TTMd-ONPs as ratiometric NIR-nanothermometers with two-photon excitation were tested with enucleated porcine eye sclera, as a real tissue model, obtaining a similar temperature relative sensitivity as in aqueous suspensions of TTMd-ONPs, demonstrating their potential as NIR-to-red/NIR nanothermometers for bio applications. In addition, it was demonstrated the key role of the hindrance in meta positions in the excimer forming process in polyhalogenated trityl radicals. For the future, exploiting different non-perhalogenated aromatic rings,[37,38] new excimer forming radicals will be synthesized aiming to increase the 2PA cross section, the photostability and the fluorescence quantum yield in the solid state, optimizing the sensing properties.

Supporting Information

Supporting Information is available from the Wiley Online Library or from the author.

Acknowledgements

N.G.-P. and D.B. contributed equally to this work. The research leading to these results received funding from the European Union in the framework of H2020-MSCA-RISE-2020, Research and Innovation Staff Exchange under a grant agreement no. 101007804 (Micro4Nano). Financial support by the MCIN/AEI of Spain (projects PID2019-105622RB-I00, 2023AEP092, PID2021-128569NB-I00, PID2022-137332OB-I00 and CEX2019-000919-M funded by MCIN/AEI/10.13039/501100011033 and by "ERDF A way of making Europe"), the Generalitat de Catalunya (SGR Cat 2021-00438), the Networking Research Center on Bioengineering, Biomaterials, and Nanomedicine (CIBER-BBN) and the Generalitat Valenciana (MFA/2022/017) is also acknowledged. This research was part of

the CSIC program for the Spanish Recovery, Transformation and Resilience Plan funded by the Recovery and Resilience Facility of the European Union, established by the Regulation (EU) 2020/2094. The MFA/2022/017 project forms part of the Advanced Materials programme supported by MCIN with funding from European Union NextGenerationEU (PRTR-C17.I1) and by Generalitat Valenciana. ICMAB-CSIC acknowledges support from the Severo Ochoa Programme for Centres of Excellence in R&D (FUNFUTURE, CEX2019-000917-S). This work had developed inside the Materials Science PhD programs of Universitat Autonoma de Barcelona and of University of Parma. Nerea Gonzalez-Pato acknowledges the financial support from the FPU fellowship (FPU17/02551) from the Spanish Ministry. J.A. is indebted to the MCIN/AEI for his Ramón-y-Cajal (RyC-2017-23500) fellowship funded by MCIN/AEI/10.13039/501100011033 and by "ESF Investing in your future". The authors also acknowledge the ICTS NANBIOSIS for the support of the Biomaterial Processing and Nanostructuring Unit (U6) at ICMAB-CSIC (https://www.nanbiosis.es/portfolio/u6-biomaterialprocessing-and-nanostructuring-unit/). This work has benefited from the equipment and framework of the COMP-HUB Initiative, funded by the "Departments of Excellence" program of the Italian Ministry for Education, University and Research (MIUR, 2018–2022). The Support from Fondazione Cassa di Risparmio di Torino through the project Visco-3D-Cell was also gratefully acknowledged. The support of the European's Union Horizon 2020 Research and Innovation program under the grant agreement no. 871124 Laserlab Europe was gratefully aknowledged. AL, FB and FT would like to acknowledge Federico Boccucci for the preliminar two-photon microscopy characterization. DB acknowledges the REFIN (Return for Future Innovation) action, an initiative co-funded by European Union and Apulian region (Italy) through the POR Puglia 2014–2020 (ID grant 2455F798). Finally, we also acknowledge support of the publication fee by the CSIC Open Access Publication Support Initiative through its Unit Information Resources for Research (URICI).

Conflict of Interest

The authors declare no conflict of interest.

Data Availability Statement

The data that support the findings of this study are available from the corresponding author upon reasonable request.

Keywords

luminescence, NIR nanothermometer, organic nanoparticles, polychlorotriphenylmethyl radicals, two-photon absorption

Received: October 7, 2023
Published online:

[1] A. Obolda, X. Ai, M. Zhang, F. Li, *ACS Appl. Mater. Interfaces* **2016**, *8*, 35472.
[2] Q. Peng, A. Obolda, M. Zhang, F. Li, *Angew. Chem., Int. Ed.* **2015**, *54*, 7091.
[3] A. Obolda, M. Zhang, F. Li, *Chinese Chem. Lett.* **2016**, *27*, 1345.
[4] Y. Tao, K. Yuan, T. Chen, P. Xu, H. Li, R. Chen, C. Zheng, L. Zhang, W. Huang, *Adv. Mater.* **2014**, *26*, 7931.
[5] G. M. Farinola, R. Ragni, *Chem. Soc. Rev.* **2011**, *40*, 3467.
[6] C. Fan, C. Yang, *Chem. Soc. Rev.* **2014**, *43*, 6439.
[7] X. Bai, W. Tan, A. Abdurahman, X. Li, F. Li, *Dye. Pigm.* **2022**, *202*, 110260.
[8] L. Chen, T. Rudolf, R. Blinder, N. Suryadevara, A. Dalmeida, P. J. Welscher, M. Lamla, M. Arnold, U. Herr, F. Jelezko, M. Ruben, A. J. C. Kuehne, *Macromolecules* **2023**, *56*, 2104.
[9] T. Li Chu, S. I. Weissman, *J. Chem. Phys.* **1954**, *22*, 21.
[10] Y. Hattori, T. Kusamoto, H. Nishihara, *Angew. Chem., Int. Ed.* **2014**, *53*, 11845.
[11] D. Blasi, D. M. Nikolaidou, F. Terenziani, I. Ratera, J. Veciana, *Phys. Chem. Chem. Phys.* **2017**, *19*, 9313.
[12] A. Bromberg, D. Meisel, *J. Phys. Chem.* **1985**, *89*, 2507.
[13] A. Bromberg, K. H. Schmidt, D. Meisel, *J. Am. Chem. Soc.* **1985**, *107*, 83.
[14] T. Okamura, K. Obi, I. Tanaka, *Chem. Phys. Lett.* **1973**, *30*, 90.
[15] M. Souto, M. V. Solano, M. Jensen, D. Bendixen, F. Delchiaro, A. Girlando, A. Painelli, J. O. Jeppesen, C. Rovira, I. Ratera, J. Veciana, *Chem. – A Eur. J.* **2015**, *21*, 8816.
[16] I. Ratera, S. Marcen, S. Montant, D. Ruiz-Molina, C. Rovira, J. Veciana, J.-F. Létard, E. Freysz, *Chem. Phys. Lett.* **2002**, *363*, 245.
[17] R. Matsuoka, S. Kimura, T. Kusamoto, *ChemPhotoChem* **2021**, *5*, 669.
[18] D. Blasi, N. Gonzalez-Pato, X. Rodriguez Rodriguez, I. Diez-Zabala, S. Y. Srinivasan, N. Camarero, O. Esquivias, M. Roldán, J. Guasch, A. Laromaine, P. Gorostiza, J. Veciana, I. Ratera, *Small* **2023**, *19*, 2207806.
[19] D. J. Naczynski, M. C. Tan, M. Zevon, B. Wall, J. Kohl, A. Kulesa, S. Chen, C. M. Roth, R. E. Riman, P. V. Moghe, *Nat. Commun.* **2013**, *4*, 2199.
[20] I. Martinic, S. V. Eliseeva, S. Petoud, *J. Lumin.* **2017**, *189*, 19.
[21] Y. Hattori, E. Michail, A. Schmiedel, M. Moos, M. Holzapfel, I. Krummenacher, H. Braunschweig, U. Müller, J. Pflaum, C. Lambert, *Chem. – A Eur. J.* **2019**, *25*, 15463.
[22] X. Wu, J. O. Kim, S. Medina, F. J. Ramírez, P. Mayorga Burrezo, S. Wu, Z. L. Lim, C. Lambert, J. Casado, D. Kim, J. Wu, *Chem. – A Eur. J.* **2017**, *23*, 7698.
[23] B. Valeur, *Molecular Fluorescence Principles and Applications*, Wiley-VCH, New York, **2001**.
[24] C. D. S. Brites, P. P. Lima, N. J. O. Silva, A. Millán, V. S. Amaral, F. Palacio, L. D. Carlos, *Nanoscale* **2012**, *4*, 4799.
[25] A. Y. Tesio, D. Blasi, M. Olivares-Marín, I. Ratera, D. Tonti, J. Veciana, *Chem. Commun.* **2015**, *51*, 17623.
[26] J. Guasch, X. Fontrodona, I. Ratera, C. Rovira, J. Veciana, *Acta Crystallogr* **2013**, *69*, 255.
[27] O. Armet, J. Veciana, C. Rovira, J. Riera, J. Castaner, E. Molins, J. Rius, C. Miravitlles, S. Olivella, J. Brichfeus, *J. Phys. Chem.* **1987**, *91*, 5608.
[28] Y. J. Bae, D. Shimizu, J. D. Schultz, G. Kang, J. Zhou, G. C. Schatz, A. Osuka, M. R. Wasielewski, *J. Phys. Chem. A* **2020**, *124*, 8478.
[29] D. Casanova, *Int. J. Quantum Chem.* **2015**, *115*, 442.
[30] A. L. Bialas, F. C. Spano, *J. Phys. Chem. C* **2022**, *126*, 4067.
[31] A. Troisi, G. Orlandi, *J. Phys. Chem. A* **2006**, *110*, 4065.
[32] M. Ghezzi, I. Ferraboschi, A. Delledonne, S. Pescina, C. Padula, P. Santi, C. Sissa, F. Terenziani, S. Nicoli, *J. Controlled Release* **2022**, *349*, 744.
[33] C. D. S. Brites, K. Fiaczyk, J. F. C. B. Ramalho, M. Sójka, L. D. Carlos, E. Zych, *Adv. Opt. Mater.* **2018**, *6*, 1701318.
[34] A. A. Kalinichev, M. A. Kurochkin, E. V. Golyeva, A. V. Kurochkin, E. Lähderanta, M. D. Mikhailov, I. E. Kolesnikov, *J. Lumin.* **2018**, *195*, 61.
[35] M. Quintanilla, M. Henriksen-Lacey, C. Renero-Lecuna, L. M. Liz-Marzán, *Chem. Soc. Rev.* **2022**, *51*, 4223.
[36] W. Xu, S. Zong, F. Shang, L. Zheng, Z. Zhang, *Photonics Res.* **2022**, *10*, 2532.
[37] D. Mesto, Y. Dai, C. N. Dibenedetto, A. Punzi, J. Krajcovic, M. Striccoli, F. Negri, D. Blasi, *European J Org Chem* **2023**, *26*, e202201030.
[38] P. Mayorga-Burrezo, V. G. Jiménez, D. Blasi, T. Parella, I. Ratera, A. G. Campaña, J. Veciana, *Chem. – A Eur. J.* **2020**, *26*, 3776.

